ENGINEERING TRANSACTIONS • *Engng. Trans.* • **61**, 2, 99–117, 2013
Polish Academy of Sciences • Institute of Fundamental Technological Research (IPPT PAN)
National Engineering School of Metz (ENIM)

Failure Analysis (Experimental and Numerical Approach) of Gas Turbine Generator Cooling Fan in Comparison between using 2types (14° and 19° Angle of Attack) of Blades

Ali JAHANGIRI[1)], Seyed Ebrahim Moussavi TORSHIZI[2)], Seyed Majid Yadavar NIKRAVESH[3)]

[1)] *Semnan University, Faculty of Mechanical Engineering*
Semnan, Iran
e-mail: a_jahangiri@sun.semnan.ac.ir

[2)] *NRI – Niroo Research Institute*
P.O. Box 14665/517, Tehran, Iran
e-mail: emoussavi@nri.ac.ir

[3)] *Power & Water University of Technology*
P.O. Box 16765-1719, Tehran, Iran
e-mail: nikravesh@pwut.ac.ir

In gas turbine power plants, a fan is used as a cooling system to dissipate generated heat in coils (copper conductors) and generator electric circuits at the end sides of its rotor. In some cases, fracture of blades causes a short circuit between rotor and stator and consequently generator explosion and financial problems. The fracture of cooling fan blades has occurred five times at the turbine side of the generator in our case of study, just 100hr after resuming operations after an overhaul.

Using numerical analysis as well as laboratory investigation – including visual inspections, metallography and SEM – can help better find failure problems that cause blade failures. A series of numerical analysis was performed to diagnose the possible cause of failure. CFD analysis is used to study the airflow distribution in order to observe probable separation phenomenon and pressure forces as they are imposed on fan blades due to operation. A finite element method was utilized to determine the stresses and dynamic characteristics of the fan blade (natural frequencies, stresses and vibrations).

Key words: fatigue failure, dimple rupture, fan blade, scanning electron microscope (SEM), resonance, fan blade angle of attack, computational fluid dynamic (CFD), finite elements.

1. Introduction

There are eleven blades on both sides of generator, which have been installed and are separated with eleven spacer pieces. Figure 1 shows the position and

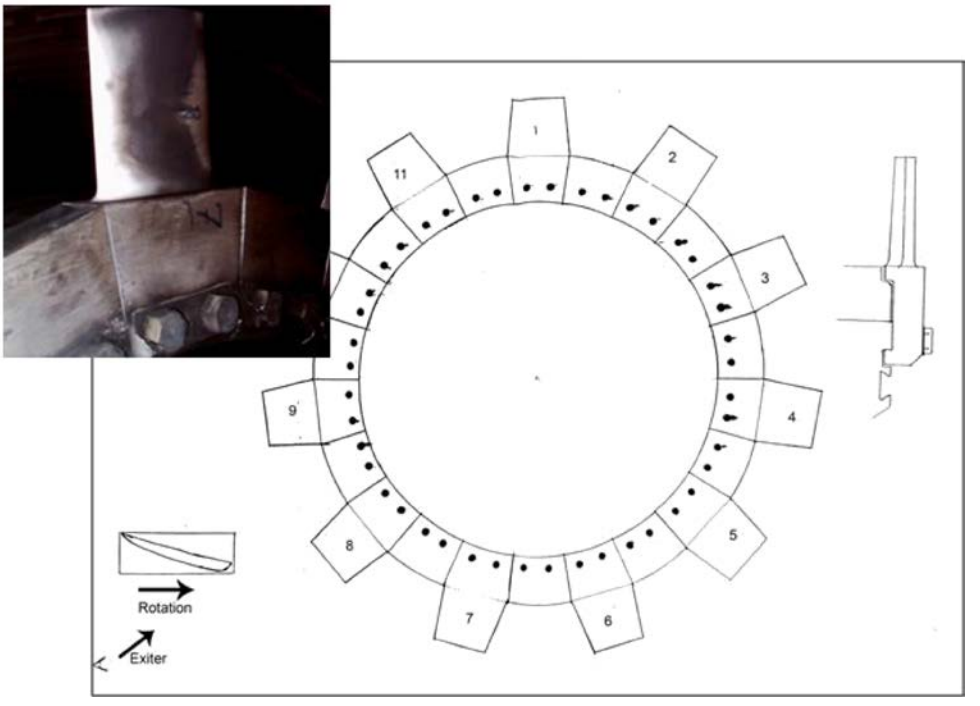

FIG. 1. Setting of blades with their spacers around a retaining ring [1, 5].

arrangement of blades and spacer pieces on a retaining ring. The axial fan has been utilized as a cooling system manufactured by GEC-ALSTHOM Belford under the following conditions; Turbine rotation = 3000 rpm; output power = 118 MW [9, 11, 12].

It must be noticed that all of the fractured blades have a 19°-angle of attack and after failure GEC-ALSTHOM replaced them by 14°-angle of attack (without a change in alloy type) in order to decrease the forces applied to the blades. The width of the 14°-blades is lower than the 19°-blades, but their length is the same. Both type of blades are compared in Fig. 2 which also defines the differences between angle and blade dimensions.

In accordance with previous studies of failure, some examples are listed below: XI *et al.* [13] investigated the failure of disk and blade for the first stage of the compressor in an aero engine. Metallurgical analysis and investigation of stress clarified that the design was not accurate, which resulted from extreme load of centrifugal bending moments and improper contact conditions.

BEISHEIM and SINCLAIR [4] and HOU *et al.* [6] performed a series of mechanical analyses and examination of a damaged blade in a gas turbine engine and utilized nonlinear finite elements to determine the stress of the blade in order to identify the cause of blade failure.

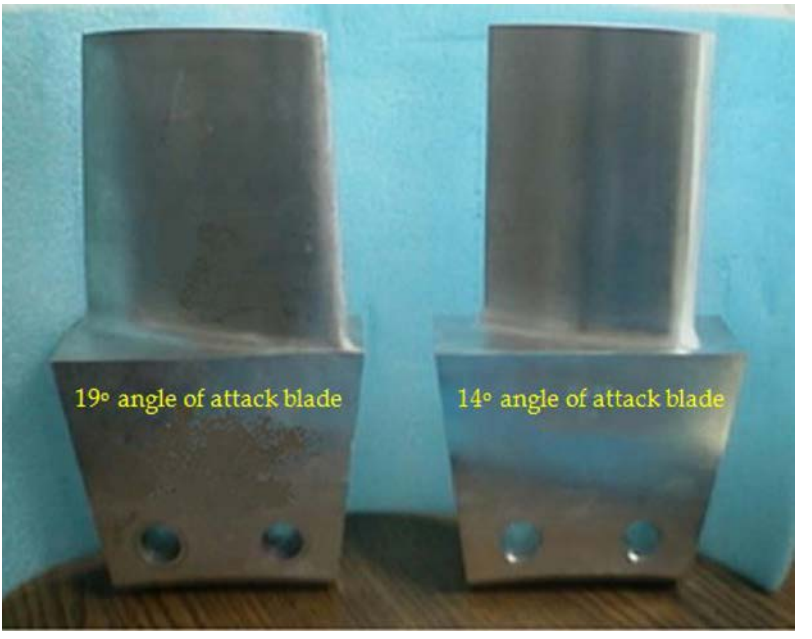

FIG. 2. Dimensional deference between 2 types of blade [5].

HUTSON *et al.* [7] verified the efficiency of a method of fracture mechanics used to model the crack growth behavior of fatigue nucleated cracks obtained under tested conditions similar to those found in turbine engine blade attachments and the calculated Crack propagation lives using stress results of FEM analysis. BARLOW and CHANDRA [3] simulated the three dimensional fatigue crack in a typical military aircraft engine fan blade attachment by Franc3D.

In the remainder of this paper, two series of analysis (laboratory investigation and Numerical) have been performed, and their results are evaluated to identify the possible causes of failure.

To study the reasons for blade fracture, this matter was reviewed and studied from different points of view as in the following (laboratory investigation):

1. Review of the history of blade repairs and/or modifications (change in blade angle of attack from 19° to 14°).
2. Material and microstructure (quantometry).
3. Metallurgical examination of fractures to identify the metallurgical mode of failure (SEM).

In the first part, studies on ruptured surfaces have shown that fracture would occur as a result of high cycle fatigue (hcf) [6]. The presented numerical research will prove this result and show that the probability of failure can be weak by changing the angle of attack from 19° to 14°.

The numerical investigations are listed below:

1. CFD analysis in order to study the imposed stresses of the fan blades due to operation.
2. Application of the finite element method for modal and harmonic analysis to compute the natural frequencies, stresses and vibration.

2. Mechanical and laboratory investigation

2.1. Visual inspection

The statistical data revealed that all of these failures happened at the first hours of operation after gas turbine repair, this means that no fracture has happened after 100 hr of operation. On opening the turbine casing, three kinds of blades (for using a 19°-attack angle) were found: A broken one, a cracked one, and blades having no failure. The failure was at the turbine side of the generator and there was no crack on the exciter side. The failure occurred at the transition section (airfoil and blade root tangency). The crack initiation point was at the central part of the airfoil on its concave surface. Some parts of the surface appeared black and pitted due to an electric spark; but, by changing the attack angle of the blades to 14° no failures have been seen. However, temperature rise in the generator casing is higher than 19° and resulted from decreasing the sucked air flow rate for generator cooling [5].

2.2. Microstructure and metallurgical investigation

The quantometry test technique is used for chemical composition of blade material specification and this composition compared with some metal alloy composition that is available in reference books. It confirms that the composition of the blade material is similar to the aluminum 2024 alloy (Table 1). Also the result of a metallurgical examination over blades shows that the blades are not produced by die casting, but rather by molding, milling, and shaping, and finally the blades surfaces would be polished. Crystals, which have been formed in the

Table 1. Chemical composition of the blade and its comparison with aluminium 2024 alloy.

Elements	Al	Zn	Si	Fe	Mn	Mg	Cu
quantometry test	Base	0.07	0.07	0.11	0.67	1.36	3.97
Al 2024 [8]	Base	–	–	–	0.6	1.5	4.4
Al 2024 [11]	Base	Max 0.25	Max 0.5	Max 0.5	0.3–0.9	1.2–1.8	3.8–4.9

blade length direction, are a proof of this claim. Heat treatment performed in this blade is T351 heating operations [9]. Some important blade and material mechanical behavior are derived and presented in Tables 2 and 3.

Table 2. Mechanical strength of aluminium 2024 [8].

Alloy	Ultimate tensile stress [9] σ_{ut}	Yield tensile stress [9] σ_{yp}	Fatigue endurance limit σ_e
Al 2024	470 MPa	325 MPa	140 MPa
Al 2024 @ Temperature 24°C	469 MPa	324 MPa	140 MPa
Al 2024 @ Temperature 100°C	434 MPa	310 MPa	140 MPa

Table 3. Mechanical properties of aluminium 2024 [8].

Alloy	Poisson's ratio Υ	Elasticity modulus E			Density P	Coefficient of thermal expansion α	Melt Point
		Tension	Shear	Pressure			
Al 2024	0.33	72.4 GPa	28.0 GPa	73.8GPa	2770 Kg/m^3	22.9 µm/m·K	638°C

2.3. Study of fracture surfaces by SEM

Generally, blade failures can be sorted into two categories [2, 10]:

1. Gradual failure in the effect of endurance (fatigue).
2. Failure in result of external material impact (dimple rupture).

It is obvious that one of the most important ways of investigating the failure pieces, is to study the failure of surfaces. This section engages with the inspection of failure surfaces and defining its result.

In order to study the failure surface and compare the quality of these two possible failure mechanisms with a standard failure handbook of this alloy, to diagnose the main reason of failure, a Scanning Electron Microscope (SEM) was employed. SEM is used to prepare the best high quality picture of a surface with the highest accuracy (scaled to $\times 1000$) for investigation of the microstructural difference between failure surface types.

In this investigation, the theory of fatigue failure and dimple rupture is considered. A 1×1 cm piece of blade alloy has been prepared and broken with a single external material impact; also, by using fractured surface of blade which has been broken in power plant, both types of fractured surface are compared with surfaces that have been shown in reference books. By comparison of Fig. 3 (the surface of a broken blade at a power plant incident) and Fig. 4 (broken in type

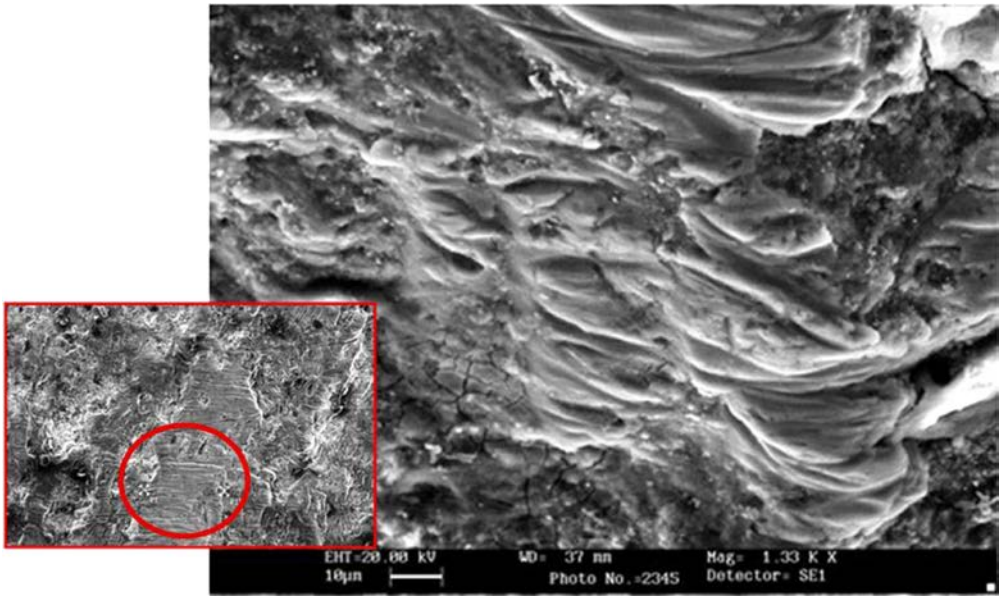

FIG. 3. Fatigue surface failure (scaled ×1330).

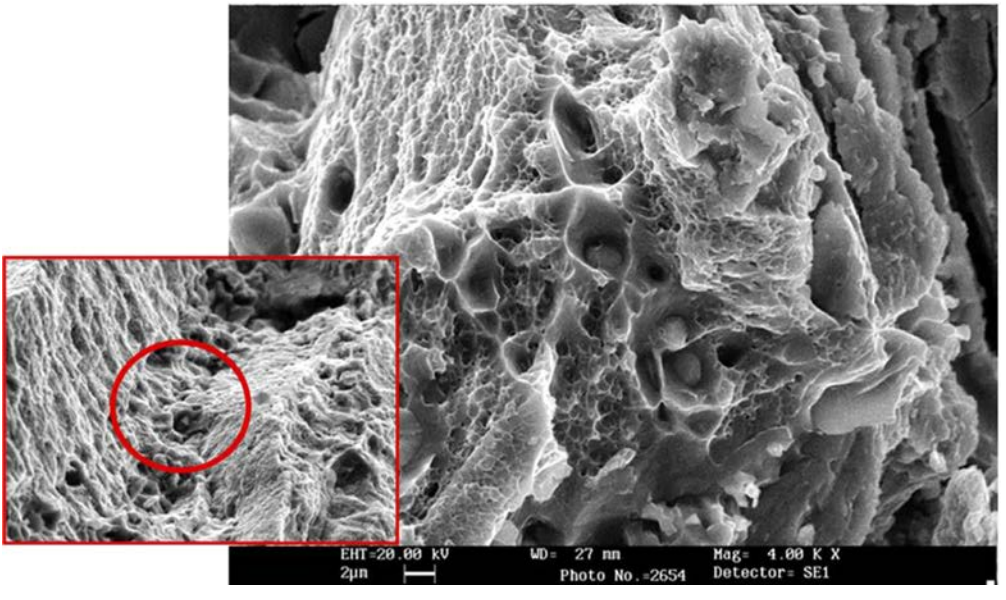

FIG. 4. Dimple rupture result of instant impact (scaled ×4000).

of dimple rupture (breaking potholes)) with reference books, it can be clearly observed that existing lines on Fig. 4 are fatigue lines. The fatigue lines show that the crack is initiated at one side and propagated with the passing of time.

Concerning a reference fatigue fracture surface, Fig. 5 shows that the final fracture occurs in accordance with crack propagation and results in periodically applied forces and fatigue.

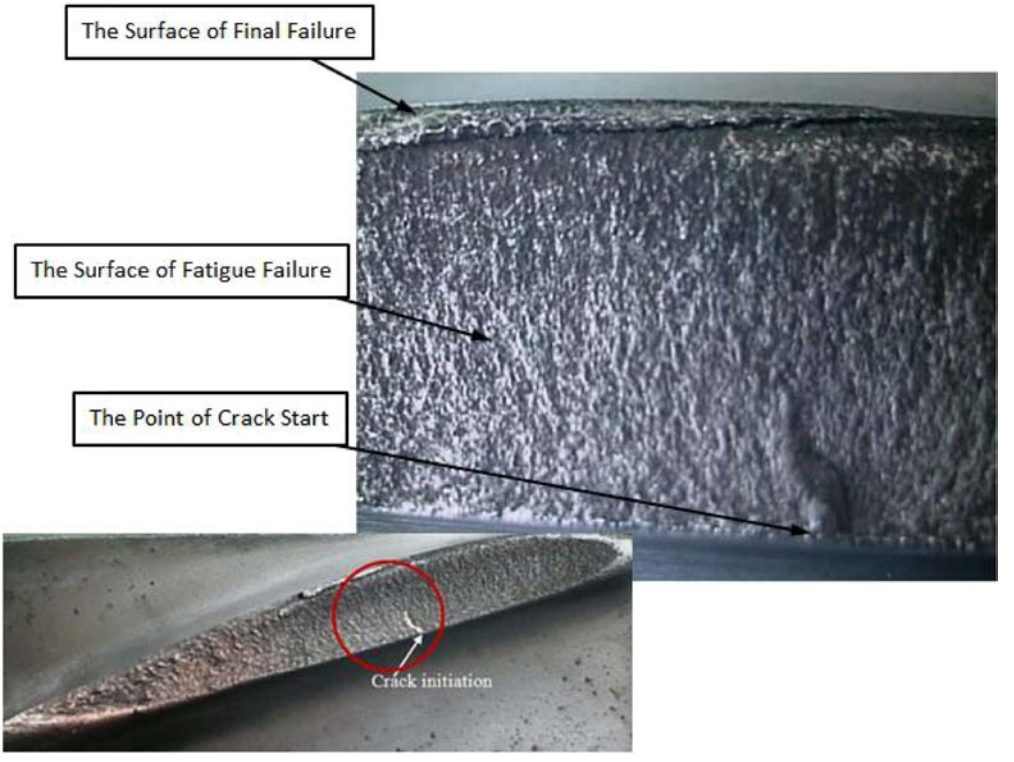

FIG. 5. Final and fatigue failure surface.

3. Numerical analysis on 14° and 19°-blades

Separation phenomenon and vortex flow are factors that may cause vibration in fan blades due to vortex flow creation, the pressure distribution (air flow forces) at two sides of fan blades change in an oscillatory way [9]. In order to study the aforementioned phenomenon, and also the distribution of air pressure forces on blade body due to operation, fan blades and their effective domain should be simulated. To do this, CFD (Computational Fluid Dynamic) code and FEM (Finite Element Method) were employed to analyze air flow distribution and vibration respectively.

Vibration due to the oscillatory change of pressure distribution may cause blade fatigue on two sides of blade [10]. Therefore the purpose of CFD analysis is to achieve an air velocity distribution around blades and also to study

air flow patterns (in order to discern probable vortex forming) and also for the determination of the force resulting from air pressure over blades. In this order after determination of 14° and 19°-blade profile is prepared by using a scanning digitizer camera with higher than micron accuracy. Then, the air passage channel and related domain modeling is necessary, which was performed by CAD software as shown in Fig. 6 and the 3-dimentional model thus obtained, is then imported to mesh generation software, which generates the meshing for the volume as shown in Fig. 7.

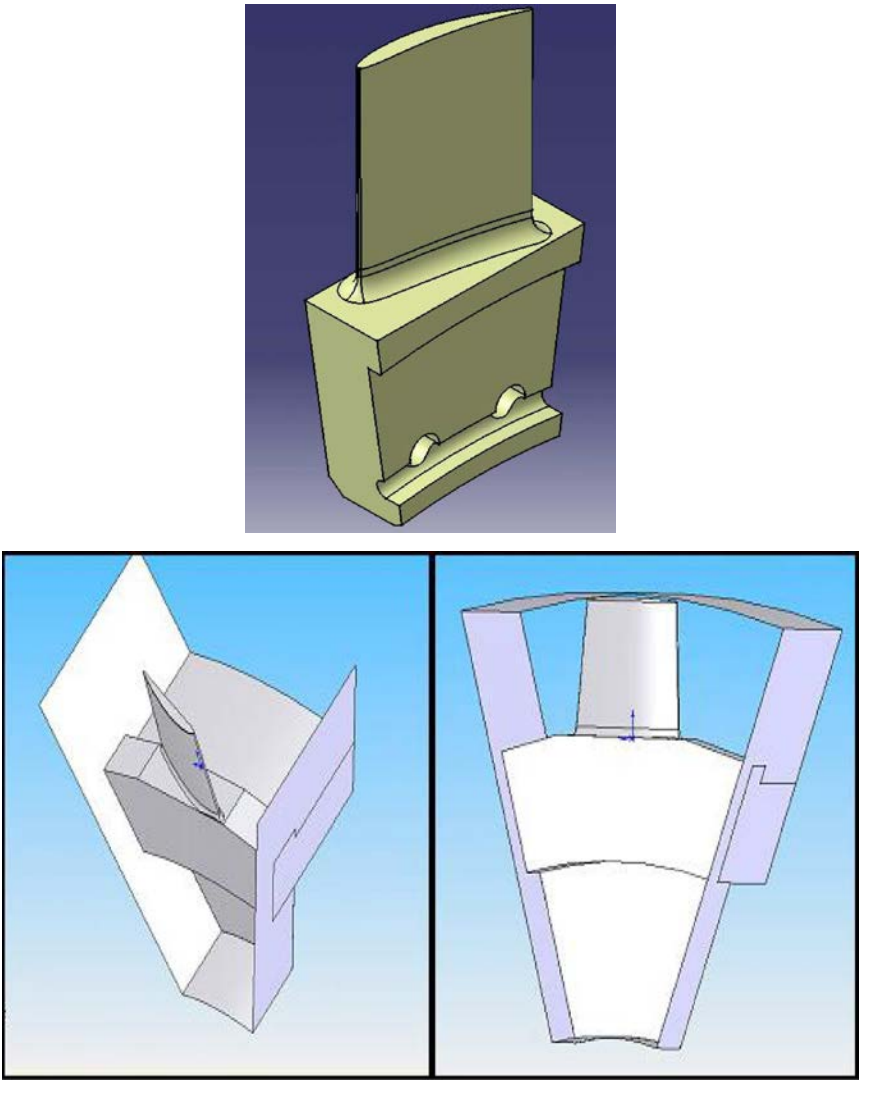

FIG. 6. 3-dimensional model of blade and related passage channel.

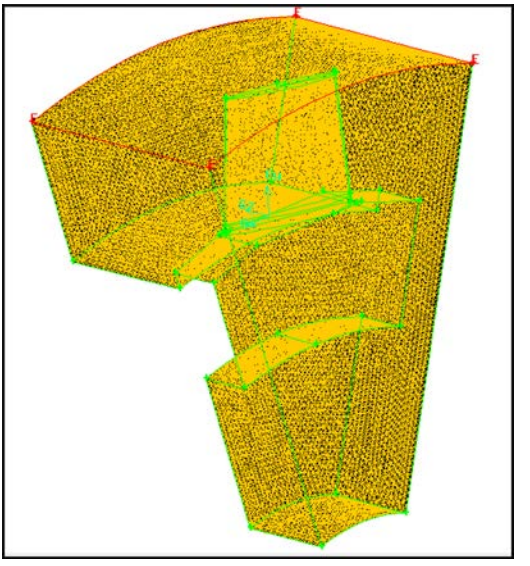

FIG. 7. Meshing domain in solution range.

3.1. Computational fluid dynamics (CFD) analysis

3.1.1. Solution procedure. Because of the turbulent action induced by high Reynolds swirling flow pattern, the standard k-ε two-equation turbulence model, the continuity and momentum are selected.

In these kinds of problems where a moving object is the cause of fluid flow, it is possible to take the rotational component of the axial velocity of air to count blade rotation (equivalent to 314.1592 rad/s as calculated: $\omega = 2\pi \times 3000$ R.P.M/60) [9, 12]. The total volumetric flow of the cooling air is 45.6 m^3/s using both type of blades, and half of that is directed towards fan at the turbine end and the other half is directed towards fan at the exciter end. At the inlet duct cross-section, the velocity of air is calculated as $V = (Q/2)/A = 16.71$ m/s (also, it should remain in mind that the area of air passage, is the difference between the channel, which is a circle with a radius of 69.6 cm, and generator shaft cross-section, which is a circle with a radius of 22.5 cm [8]). Air pressure is uniform for all of the outlet area and along its duct, which will be approximately equal to ambient pressure. For reduction of the solution domain to reach the least logical possible domain, a periodic analysis would be used.

3.1.2. Analysis of flow field and pressure. As seen in Fig. 8a and b, in both blade types the airflow pattern is typical. It is observed that the path lines are completely tangent over the blades and the separation phenomenon has not incurred.

a)

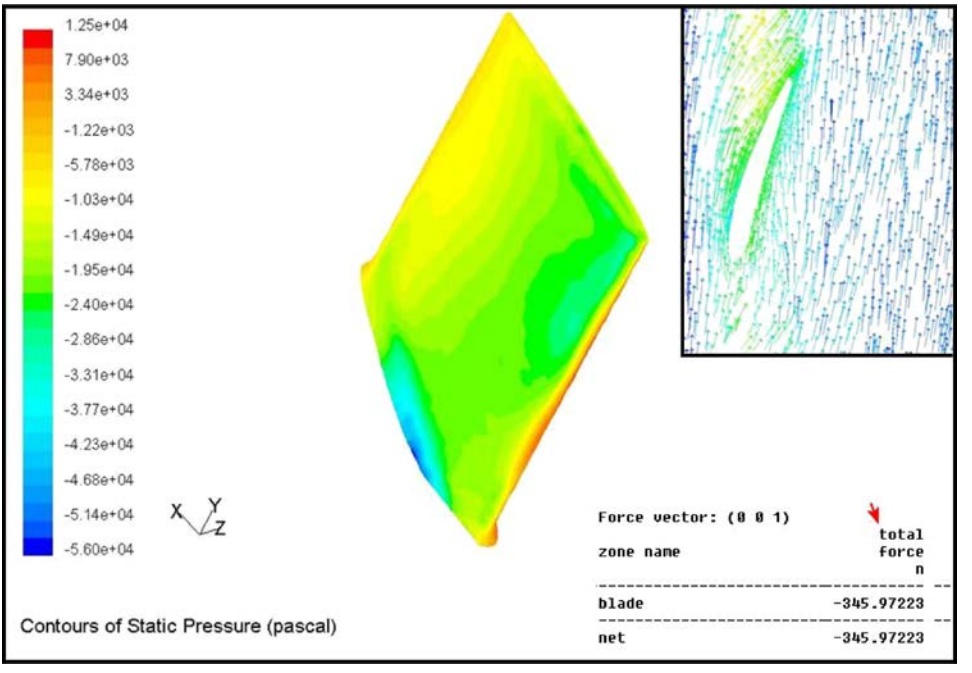

b)

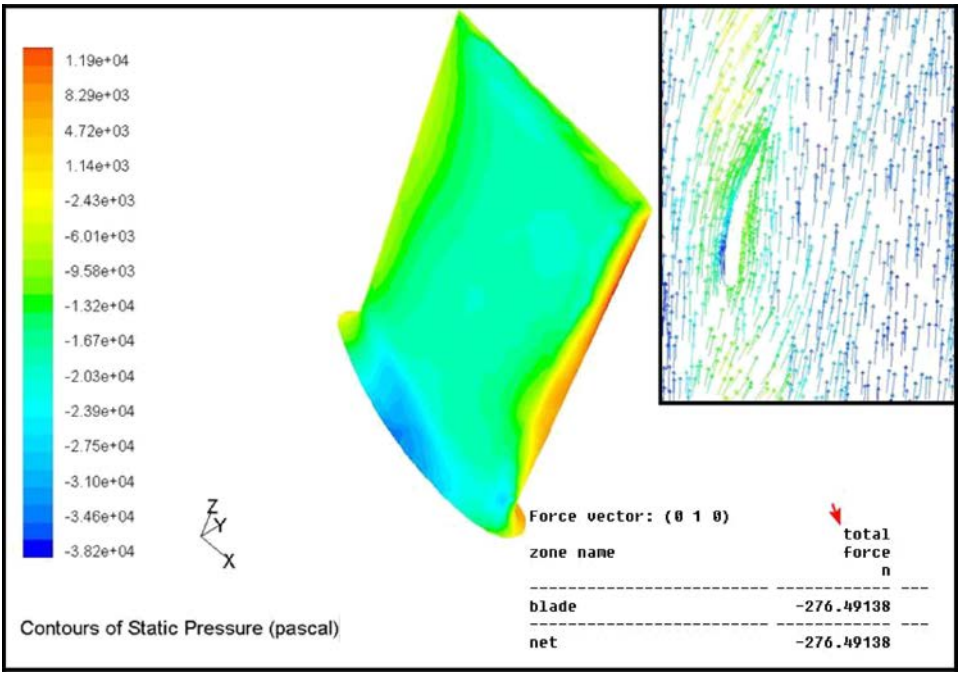

FIG. 8. a) Pressure contour and velocity vectors passed over 19°-angle of attack blade, and b) pressure contour and velocity vectors passed over 14°-angle of attack blade.

The air pressure distribution can also been seen over the blades in these two figures. The maximum absolute value of pressure that is imposed on the 19°-angle of attack blade reaches 56 kPa on the bottom of the blade surface and the resultant force over the blade is approximately equal to 346 N. The results of tension for the mentioned force, is less than the amount that solely causes breaking of the blade.

Also in the 14°-blade, the maximum pressure at the bottom of the blade reaches 39 kPa and is even less than for the 19°-blade.

While the 19°-angle of attack blade has been changed with a 14°-blade, the amount of force imposed on the blade would decrease nearly 20% and is reduced from 346 to 276 N, then, these forces caused by air flow are not enough to cause blade rupture.

3.2. Finite element method analysis (FEM)

In order to determine the applied stresses on the blade and investigate the possibility of its failure resulting from resonance, the finite element method was used. A 3D numerical model of a gas turbine generator cooling fan blade was constructed and meshed to get the FEM of a single blade. The FEM has a structured mesh with ninety twenty-node solid elements to employ structural analyses, which have compatible displacement shapes and are well suited to model curved boundaries due to the complexity of the geometry. This blade was analyzed under two followings categories of FEM analysis [4, 5]:

1. Modal analysis;
2. Harmonic analysis.

The modal analysis on natural frequency and the harmonic analysis was done based on different excitation frequencies.

3.2.1. Modal analysis. First, the amount of bolt tightening and clearance between the blade root and retaining ring were modeled as constraints and their affect on the first natural frequency of the blade was studied as shown in Table 4. To evaluate these conditions, four different constraints were investigated for both the 19° and 14°-blade:

1. Just points around the bolts are assumed to be fixed.
2. All points from the surface of blade's root to the bolts are assumed to be fixed.
3. The contact surface with the retaining ring, as well as points mentioned in item two, are assumed to be fixed
4. The whole part of blade's root are assumed to be fixed in all directions.

Table 4. Calculated natural frequency in the first mode for four-bolt tightening states.

Bolts tightening state number	First Natural Frequency (Hz) 19° blade	First Natural Frequency (Hz) 14° blade
State No 1	480.97	367
State No 2	489.58	375.3
State No 3	513	394.9
State No 4	537.88	413.49

Based on Table 4, the first natural frequency of the blade for the fourth assumed constraint in both type of blades is bigger than the others.

The natural frequency in the five modes for these four states were calculated. Table 5 shows the natural frequencies for the fourth constraint in both type of blades.

Table 5. Calculated natural frequency in the 5 modes for 19° and 14°-blade.

Mode shape number	Natural Frequency (Hz) 19° blade	Natural Frequency (Hz) 14° blade
Mode No 1	537.88	413.49
Mode No 2	1339.8	1232.6
Mode No 3	2693.8	2365.9
Mode No 4	2637.1	2794.5
Mode No 5	3879.5	3837.1

In Fig. 9 the displacement of the tip of both blades at the first modal shape has been represented with Finite Element modeling. With respect to the fact that the first natural frequency of the 19°-angle of attack blade in the fourth state (538 Hz) was very close (almost within a 2% relative difference) to the frequency of the exciting force caused by shaft rotation (11 blades $\times$ 50 rad/s = 550 Hz) and therefore the incurrence of resonance in the above conditions is very probable. This state has been selected for finite element harmonic numerical simulation. Whereas 19°-blades are replaced with 14°-blades such that the natural frequency in the fourth mode (413.49 Hz) will not be close (with 33% relative difference) to exciting frequency and therefore resonance conditions will not occur.

3.2.2. Harmonic analysis In harmonic analysis, the frequency of external forces (air flow and shaft rotating force) acting on the blades, gradually increases, (from zero to 1000 Hz) then, domain, difference shapes of vibrations and tension

a)

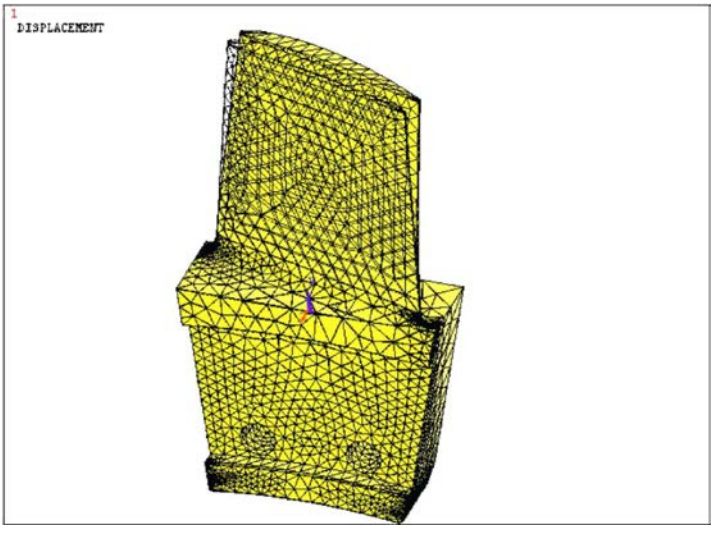

b)

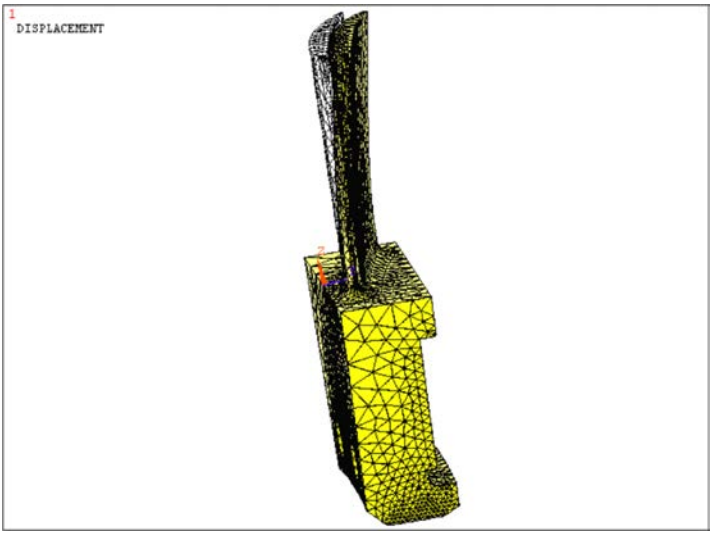

FIG. 9. a) Blade tip displacement at the first modal shape for a 19°-angle of attack blade, and b) blade-tip displacement at the first modal shape for a 14°-angle of attack blade.

result of these acting external forces with, changing in blade type, account for the various frequencies.

3.2.3. Harmonic analysis for 19°-blade. From CFD analysis force acted by air flow on 19°-blade was calculated about 346 N. By acting these external forces

to blade in the various frequencies (between 0 to 1000 Hz), blade tip oscillation domain (blade tip displacement), is accounted with finite element analysis. The blade-tip displacement for these conditions is shown in Fig. 10.

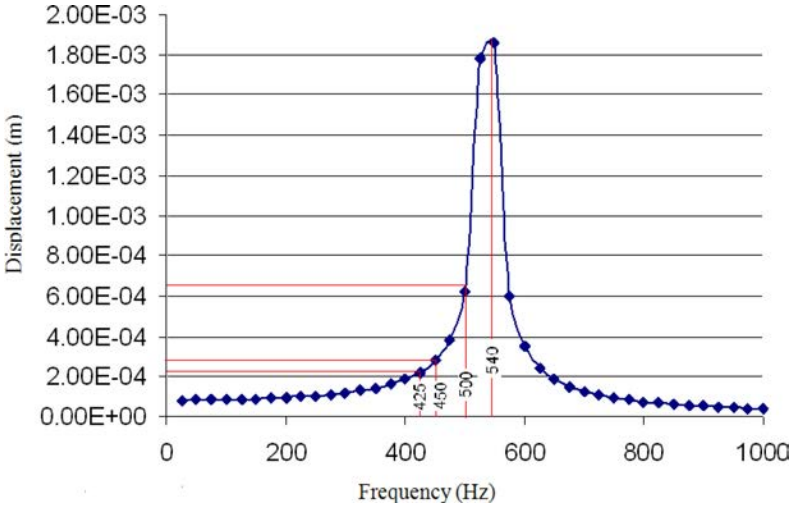

FIG. 10. 19°-blade-tip displacement at various frequencies in the first mode of vibration.

As seen, at a frequency of 50 Hz, the blade tip displacement reaches around 82 μm, and this value grows with increasing frequency up to the extent of 425 to 450 Hz and reaches 220 to 280 μm.

In the vicinity of the first natural frequency, displacement intensely increases and reaches nearly 1.8 mm and thereafter with increasing frequency, the blade tip displacement again decreases intensively.

According to Fig. 10, the resonance condition is imminent when the blade has been excited to a frequency of 550 Hz, that is, near to the first natural frequency. The blade will have been vibrated intensely in this condition and as shown in Fig. 11, the von Mises stress at sensitive spaces of blade (bade root) reaches 236 MPa.

Referring to Table 2, it is obvious that tension with an amount of 236 MPa is far less than any mechanical strength of an alloy except in the fatigue endurance limit, in other words, the blade material should be able to endure any forced statistical loads even at resonance state.

The maximum amount of von Mises stress is larger (68%) than fatigue endurance limit [8, 11] (236 MPa $>$ 140 MPa), therefore, when the blade encounters the fatigue condition at resonance state, the 19°-blade is not be able to endure the fatigue condition infinitely and blade fracture will be unavoidable.

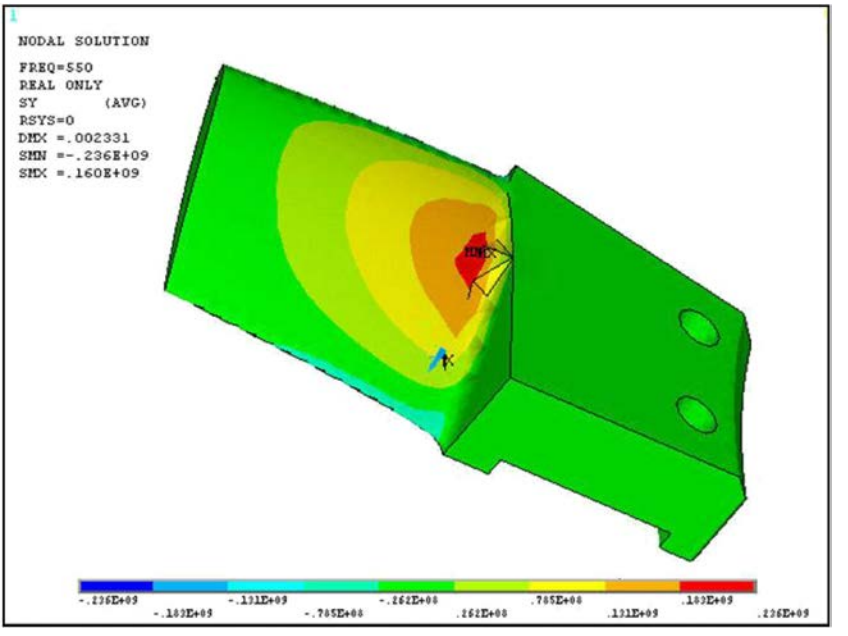

FIG. 11. Contours of the computed Von Mises stress distribution on 19°-blade at a frequency of 550 Hz.

3.2.4. Harmonic analysis for 14°-blade. From CFD analysis the force acting by air flow on the 14°-blade was calculated to be about 276.5 N. By acting these external forces on the blade at various frequencies (between 0 to 800 Hz), the blade-tip displacement is accounted with finite element analysis. The blade-tip displacement for these conditions is shown in Fig. 12.

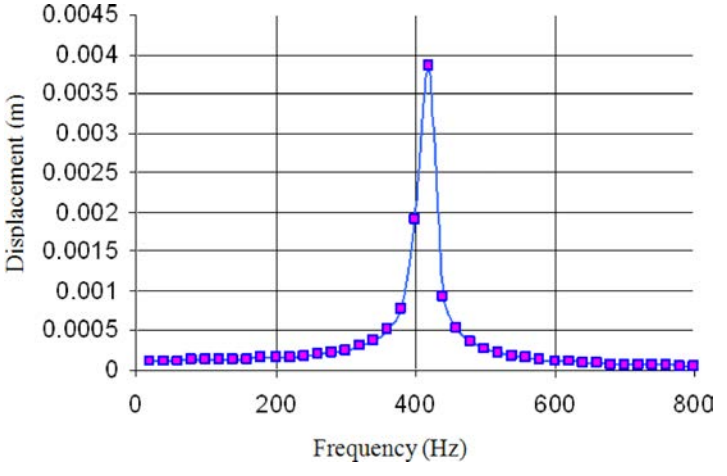

FIG. 12. 14°-blade-tip displacement at various frequencies in first mode of vibration.

As seen, at a frequency of 420 Hz the blade tip displacement reaches a maximum quantity (about 4 mm) because the frequency of 420 Hz is the closest value to the first natural frequency of 14°-blade (413.49 Hz). This amount of displacement (4 mm) is even more than for the 19°-blade in the vicinity of its first natural frequency (1.8 mm).

Notice from Fig. 12 that the frequency resonance condition happening at 420 Hz is imminent. The blade will be vibrated intensively in this condition and, as seen in Fig. 13, the von Mises stress at sensitive spaces of the blade (blade root) reaches 388 MPa. So again when the 14°-blade encounters the fatigue condition at resonance state, it was not be able to endure the fatigue condition infinitely and blade fracture will be unavoidable.

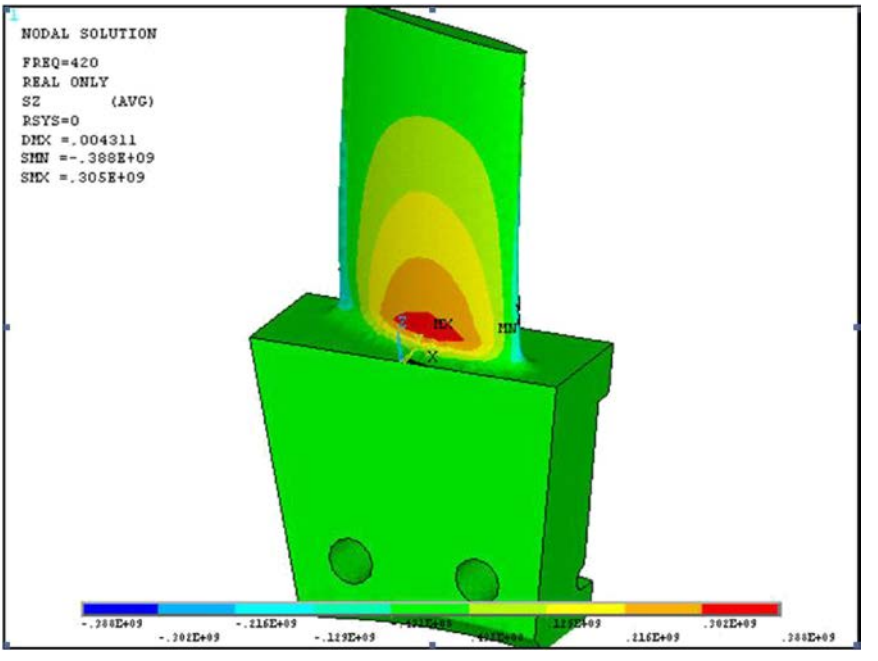

Fig. 13. Contour of computed von Mises stress distribution on a 14°-blade at a frequency of 550 Hz.

Nevertheless, as seen in Fig. 10, when the blade is excited at a frequency of 550 Hz, which is the frequency of the exciting force caused by shaft rotation, the 14°-blade tip displacement, will be less than 160 μm. Therefore, the resonance state will have not happened in this situation and the von Mises stress encountered by the 14°-blade root will be less than 10 MPa, which is small enough to be negligible. Blade failure will never been occurred for the 14°-blade in this situation.

4. Results and discussions

The results listed below have been taken from visual inspection and reports.

Measured dynamic stresses at 3000 rpm, (50 Hz frequency of power plant generators) for both 14° and 19°-blades, [5] compared with the yield stresses (presented in Table 2) and show that the stresses imposed on the blade are much lower than yield stresses and therefore there is no possibility of blade failure in normal operating conditions.

Cracking started from one or more points at the middle of the concave surface of the blade (having higher roughness can cause the crack on the surface of the blade) and this may be a reason to take the blade apart. The mentioned problem results from the effect of oscillatory loading being applied to the blade.

By changing the attack angle of the blades to 14°, no failures were observed. However, the rising of temperature in the generator casing was higher than 19°-blades. This results from a lower rate of sucked air flow for generator cooling for the 14°-blades. Since both type of blade are installed on the same shaft of the generator and rotate with the shaft, the fan rotation power is equal in both cases. However, the sucked air in the 14°-blade fan would be less than the other, and hence, the net power output is less and results in lower efficiency. For troubleshooting and to increase the sucked air flow for 14°-blades, using some extra guide blades has been proposed, as shown in Fig. 14.

Fig. 14. Extra guide blades for increasing the sucked air flow in the use of 14°-blades [5].

To investigate the cause of 19°-blades failure and having no failure in 14°-blades, SEM inspection and numerical analysis has been used as described below:

1. Study of ruptured surfaces by SEM and microstructure difference between fatigue failure and dimple rupture shows that there is no possibility of a collision of a large external object and its instantaneous rupture.

2. Distribution of flow, pressure and applied air flow forces on blades which have been modeled with CFD simulation, sustained that the forces were not enough to cause the blade rupture.
3. With respect to the obtained results from CFD and FEM, these analyses prove that the value of normal stress in most of conditions for 19° and 14°-blades is about 10 MPa, except for the resonance state.
4. In the case of applying a force with a frequency of around 550 Hz, the 19°-blade will be exposed to a resonance frequency (as a result of unsuitable blade installation, the resonance condition is probable) and because of applying stress at range of 160–236 MPa periodically and exceeds the endurance limit of the material (Al 2024 fatigue endurance limit $\sigma_e = 140$ MPa as presented in Table 2) will reduce the working life of the blade and cause failure after some cycles.
5. In the case of applying a force with a frequency of around 550 Hz, the 14°-blade will not be exposed to the resonance condition and because of applying stress at about 10 MPa, blade failure never occurs.

5. Conclusion

In accordance with the fracture of the 19°-blades, which occurred five times in the case of our study after overhaul and after less than 100 hr of operation, the investigation of the reason of fractures were necessary. By utilising a laboratory investigation (reports and SEM) and computational inspection (CFD and FEM), it is clear that the installation conditions (applied torque on bolts and nuts) were the main reason of failure.

To achieve a high accuracy in computations, the "ATOS" which is a new method based on 3D digital photography has been used for blades modeling. The results obtained from the CFD analysis have shown that the maximum stress, caused by rotation and air pressure forces on blades, is much lower than the material yield tensile strength.

Modal and harmonic analysis of the blade with FEM has indicated that the 19°-blades natural frequency is too close to the operational frequency of blades. It means that any changes in blade installation conditions cause the blade natural frequency to be similar to the operational frequency and consequently causes resonance phenomena. Because of the applied periodic stress that exceeds the endurance limit of the material, it will reduce working life of the blade and lead to failure after some cycles.

Study on fracture surfaces and results obtained from FEM show that the fracture of 19°-blades occurs in accordance with fatigue where there is resonance phenomena and crack propagation.

The natural frequency of the 14°-blades is not close to the blade's operational frequency and thus will not be exposed to a resonance condition and because of applying stress about 10 MPa, blade failure never occurs.

Acknowledgment

The authors gratefully acknowledge the office of gifted students of Semnan University for financial support.

References

1. Alsthom Company report in conjunction with some Gas Power Plants (1997).
2. Anderson L., *Fracture mechanics fundamental and applications,* CRC Press, 9780849316562, Colorado, USA (1995).
3. Barlow K.W., Chandra R., *Fatigue crack propagation simulation in an aircraft engine fan blade attachment*, Int. J. Fatigue, **27**, 1661–1668, 2005.
4. Beisheim J.R., Sinclair G.B., *On the three-dimensional finite element analysis of dovetail attachment*, [in:] *Proceedings of ASME Turbo Expo* 2002, Amsterdam, The Netherlands (2002).
5. Failure analysis report of Iran-Montazer-Ghaem units 2, 4 & 6. Iran Power Plant Repair Co, (2003–2004).
6. Hou J., Bryon J.W., Ross A., *An investigation of fatigue failures of turbine blades in a gas turbine engine by mechanical analysis*, Engineering Failure Analysis, **9**, 201–211, 2002.
7. Hutson A., Nicholas T., Johnc R., *Fretting fatigue crack analysis in Ti-6Al-4V*, Int. J. Fatigue, **27**, 1582–1589, 2005.
8. Joseph R., *ASM Specialty Handbook*, Aluminum and aluminum Alloys, ASM International, 087170496X, USA (1993).
9. Moussavi Torshizi S.E., Yadavar Nikravesh S.M., Jahangiri A., *Failure analysis of gas turbine generator cooling fan blades*, Engineering Failure Analysis, **16**, 1686–1695, 2009.
10. Paris P.C., Gomez M.P., Anderson W.E., *A rational analytical theory of fatigue*, Trend Eng., **13**, 1, 9–14, 1961.
11. Poursaeidi E., Salavatian M., *Failure analysis of generator rotor fan blades*, Engineering Failure Analysis, **14**, 851–860, 2007.
12. Poursaeidi E., Salavatian M., *Fatigue crack growth simulation in a generator fan blade*, Engineering Failure Analysis, **16**, 888–898, 2009.
13. Xi N.S., Zhong P.D., Huang H.Q., Yan H., Tao C.H., *Failure investigation of blade and disk in first stage compressor*, Eng. Fail Anal., **7**, 385–392.
14. http://www.cfg.cornell.edu/software/software.htm.

Received June 12, 2012; revised version February 2, 2013.

ENGINEERING TRANSACTIONS • *Engng. Trans.* • **61**, 2, 119–136, 2013
Polish Academy of Sciences • Institute of Fundamental Technological Research (IPPT PAN)
National Engineering School of Metz (ENIM)

An Experimental Study on Rate Sensitivity of J-Integral and its Evaluation by Small Punch Test for TRIP Steel

Leishi SHI[1)], Takeshi IWAMOTO[2)], Shinya HASHIMOTO[3)]

[1)] *Graduate School of Engineering, Hiroshima University*
1-4-1 Kagamiyama, Higashi-Hiroshima, Hiroshima, 739-8527 Japan
e-mail: m124742@hiroshima-u.ac.jp

[2)] *Institute of Engineering, Hiroshima University*
1-4-1 Kagamiyama, Higashi-Hiroshima, Hiroshima, 739-8527 Japan

[3)] *SUZUKI Motor Corporation*
300 Takatsuka, Minami, Hamamatsu, 432-8611 Japan

Recently, much attention has been paid to TRIP steel since it indicates both high ductility and strength by strain induced martensitic transformation. This transformation allows TRIP steel to offer larger energy absorption than other steel at the same strength level. Therefore, it is expected to be applied to automobiles as security components that absorb energy upon collision. To produce the best performance of TRIP steel, the J-integral of TRIP steel should be investigated with respect to a various deformation rates for an evaluation of energy absorption. In the present study, the three point bending (3B) test is conducted for investigating the J-integral until the crack growth of TRIP steel. Then, in order to determine the energy absorption characteristic by the J-integral value at various locations in the components of TRIP steel, the size of the specimen should be very small. Thus, an SP test is introduced and conducted by using the newly established apparatus based on the SHPB method. By using the result of the SP test in conjunction with the result of a 3B test, the evaluation of the J-integral of TRIP steel subject to various deflection rates is attempted. The correlation between the J-integral and the equivalent fracture strain of the SP test for TRIP steel is challenged to be redefined.

Key words: TRIP steel, energy absorption, J-integral, rate sensitivity, small punch test, SHPB method.

1. Introduction

TRIP steel indicates high ductility, toughness and excellent energy absorption under plastic deformation by strain-induced martensitic transformation (SIMT) [1]. Recently, in order to improve passenger safety and reduce weight